

The mid–infrared emission of Seyfert galaxies. A new analysis of ISOCAM data¹

C. Ramos Almeida¹, A.M. Pérez García¹, J.A. Acosta-Pulido¹, and J.M. Rodríguez Espinosa¹

ABSTRACT

We present mid–infrared data of a sample of 57 AGNs obtained with the instrument ISOCAM on board the satellite ISO. The images were obtained through the LW2 (6.75 μm) and LW7 (9.62 μm) filters. This is a new analysis of Clavel et al. (2000) galaxy sample, which is divided into 26 type 1 (≤ 1.5) and 28 type 2 (> 1.5) Seyfert galaxies, plus three QSOs. The spatial resolution of the images allow us to separate the nuclear and the extended contributions to the total emission after decomposing the brightness profiles into different morphological components. The most common components are a central point source (identified as the active nucleus) and an exponential disk. In some cases a bulge, a bar or a ring are needed. The relative contribution of the nucleus to the total emission appears larger in Seyfert 1 than in Seyfert 2. This result confirms that both types of Seyfert galaxies are different in the mid-infrared wavelength range and supports the existence of a structure which produces anisotropic emission in this wavelength range. We have also explored correlations between the mid-infrared and the radio and X–ray wavelength ranges. The well established radio/infrared correlation is maintained in our sample for the global emission of the galaxies. If only the nuclear infrared emission is considered then a non–linear correlation is apparent in the luminosity–luminosity scatter diagram. The ratio between the intrinsic hard X–ray and the nuclear mid-infrared emission presents large scatter and slightly larger values for type 2 Seyfert galaxies. These results seem to be consistent with the presence of a clumpy dusty torus surrounding the active nucleus.

Subject headings: galaxies: active — galaxies: Seyfert — galaxies: nuclei — infrared: galaxies

¹Instituto de Astrofísica de Canarias (IAC), C/Vía Láctea, s/n, E-38200, La Laguna, Tenerife, Spain. cra@iac.es, apg@iac.es, jap@iac.es, and jre@iac.es

¹Based on observations with ISO, an ESA project with instruments funded by ESA Member States (especially the PI countries: France, Germany, the Netherlands and the United Kingdom) and with the participation of ISAS and NASA.

1. Introduction

Despite the broad variety of type of objects included under the denomination of Active Galactic Nuclei (AGN), it seems to be possible to explain all of them under a common scenario, the so called Unification Models. The most successful models for the unification of Seyfert galaxies predict the existence of a blocking structure surrounding the nucleus (Antonucci 1993). This structure is likely a dusty torus, whose size and structure is still a matter of debate (Fritz et al. 2006; Hönig et al. 2006). According to this, type 1 and 2 Seyfert galaxies (hereafter Sy1 and Sy2, respectively) are proposed as the same kind of objects but viewed at different angles: Sy1 are observed close to face-on such that we have a direct view of the nucleus and the Broad emission Line Region (BLR), whereas the Sy2 are seen at an inclination such that our view is blocked by the optically thick dusty torus. The dust grains in the torus will absorb the UV photons from the central engine and after reprocessing the radiation will appear as strong emission in the infrared range. In particular, the mid-infrared emission is produced by a mixture of stochastic heating from Polycyclic Aromatic Hydrocarbon (PAHs) and thermal emission from very small dust grains at high temperatures. Active galaxies are significantly stronger radiators in the mid-infrared than non AGN-dominated galaxies (Spinoglio & Malkan 1989; Rowan-Robinson & Crawford 1989; Fadda et al. 1998; Pérez García & Rodríguez Espinosa 2001). Hence, this spectral range seems a natural window in which to study the properties of such a structure.

The mid-infrared spectra of Sy1 and Sy2 galaxies present important differences: whereas Sy1 spectra are characterized by a strong continuum with only weak emission features from PAH bands, most Sy2 display a weak continuum but very strong PAH emission bands (Clavel et al. 2000). Despite the strong dilution by the nuclear continuum in the case of Sy1, both types 1 and 2 share similar PAH luminosities. This molecular emission results unrelated to the nuclear activity, and arises in the interstellar medium of the underlying galactic bulge. The majority of dusty torus models predict different mid-infrared spectra for type 1 and 2 objects. In case of Sy1 the silicate feature at $10\ \mu\text{m}$ is expected in emission, as recently confirmed with instruments on board of the Spitzer satellite (Siebenmorgen et al. 2005). In contrast, for Sy2 this feature is observed in absorption (Clavel et al. 2000; Jaffe et al. 2004).

In this paper, we analyze mid-infrared images of a sample of Seyfert galaxies. The data sample practically coincides with the previously studied by Clavel et al. (2000), in which the images are complemented by spectra obtained with the instrument ISOPHOT-S (Lemke et al. 1996). Our main goal is to isolate the nuclear emission of the galaxies in the sample, and provide a better estimate of the active component. This new analysis of the data can be used for testing the unification models. In this line we have investigated correlations with photometric data obtained in different spectral ranges, namely radio and hard X-rays.

2. ISOCAM Data

We analyzed the mid-infrared morphology of a sample of AGNs, mostly Seyfert galaxies. These data were taken as part of the ISO Guaranteed Program *Seyfert 1 and Seyfert 2* lead by J. Clavel. We have selected this dataset because it was taken in a homogeneous way, with all the exposures obtained in the same mode and keeping the same instrumental configuration (pixel scale and filters). Morphological classification, Seyfert type, spectroscopic redshifts and observational data (exposure and observation time) are reported in Table 1. The sample was originally drawn from the CfA hard X-ray flux limited complete sample (Piccinotti et al. 1982), but lacks the most well known objects (e.g. NGC 4151 or NGC 1068) which were obtained within the frame of other ISO guaranteed time programs. The sample is about equally divided into 26 Sy1 (≤ 1.5) and 28 Sy2 (> 1.5), plus a starburst galaxy and three QSOs. Taking into account only the Seyfert galaxies, the mean and *rms* of the redshift distributions are 0.023 ± 0.014 and 0.016 ± 0.011 for Sy1 and Sy2, respectively. The mean values are not significantly different, considering the width of the distributions, clarifying that the results presented in this paper are not a consequence of differences between Sy1 and Sy2 redshift distributions. In addition to this, we have compiled the total H magnitudes for all Seyferts in the sample from The Two Micron All Sky Survey (2MASS), in order to derive their luminosity distributions. The mean $\log(L_{TOT}[\text{H}])$ are 44.81 ± 0.39 and 44.72 ± 0.42 , indicating that Sy1 and Sy2 luminosity, and consequently, mass distributions are very similar. The images were obtained using ISOCAM, the mid-infrared camera (Cesarsky et al. 1996) on board of the ISO spacecraft (Kessler et al. 1996). The ISOCAM images are formed by an array of 32x32 pixels, with a pixel size of 3 arcsec. The employed filters were LW2 (5-8.5 μm , covering PAHs emission) and LW7 (8.5-10.7 μm , including the silicate band), which provide an effective resolution on the diffraction limit of FWHM=3".8 and 4".5, respectively. Reduced data were retrieved from the ISO data archive².

3. Data Analysis

3.1. Brightness profile decomposition

We performed an isophotal analysis of the images in both filters to obtain the surface brightness profiles, by azimuthally averaging over elliptical annuli. We fitted the isocon-

²<http://www.iso.vilspa.esa.es/ida/>

tours of surface brightness with the ELLIPSE task in IRAF³, which employs the algorithm described in Jedrzejewski (1987). The spatial interval between two consecutive isophotes chosen was equal to the pixel size in all cases. Given the limited spatial resolution and the relatively small field of view of the camera, the brightness profiles are limited to a maximum of 15 data points, which means a relatively poor sampling of the profile. We subtracted the sky background emission, estimated as the median background value for each image. As a first approach, we assume that the profiles are the sum of two contributions: a nuclear component modeled with a Gaussian PSF of FWHM equals to 2 pixels⁴, and central amplitude as free parameter plus an exponential component with two free parameters (central amplitude and length scale). Using this simple model we were able to reproduce correctly the brightness profiles for about half of the galaxies in our sample. In the rest of cases we could not successfully reproduce the brightness profiles, and extra components had to be introduced in order to improve the fit. The extra components are a bulge described as a Sersic’s law; a ring described by a Gaussian profile (Buta 1996):

$$I_{ring}(r) = I_{ring}^0 \exp\left[-\frac{1}{2}\left(\frac{r - r_{ring}}{l_{ring}}\right)^2\right],$$

where I_{ring}^0 is the amplitude, r_{ring} is the center, and l_{ring} is the width; or a flat bar profile (Prieto et al. 1997):

$$I_{bar}(r) = \frac{I_{bar}^0}{1 + \exp[(r - r_{bar})/l_{bar}]},$$

where I_{bar}^0 is the amplitude, r_{bar} is the length, and l_{bar} is the downward gradient.

In all cases, the fits were performed with the criterium of minimum number of components and consistency between both filters. Whenever bars or rings were employed in the fitting, we also looked at the ellipticity and orientation of the isophotes searching for abrupt changes coincident with the position of these components. However, the limited resolution of our imaging prevents a fully reliable component identification. In addition to this, we used as a guideline the morphology of the galaxies in the visible (WFPC2/HST) from Malkan et al. (1998) and in the near-infrared (NICMOS/HST) from Hunt & Malkan (2004), although in some cases we fit nuclear bars that do not agree with the optical classification, or rings that reproduce spiral arms, as in the case of NGC 1241. The maximum number

³IRAF is distributed by the National Optical Astronomy Observatories, which are operated by the Association of Universities for the Research in Astronomy, Inc., under cooperative agreement with the National science Foundation. <http://iraf.noao.edu/>

⁴Here we assumed that the nominal spatial resolution cannot be achieved due to insufficient sampling of the PSF. The width of the profile for a point source should correspond to the minimum sampling criterium, *i.e.* 2 pixels or equivalently 6".

of fitted parameters in our fits was seven. The fitting procedure looks for minimization of the Chi-Square function formed by the squared difference between the observed and model profile, both in logarithmic scale. The multidimensional minimization of the merit function is reached using the downhill simplex method. This is the same fitting technique employed in Melo et al. (2002) in the study of NGC 253. In Table 2 we report the fit parameters and their corresponding errors for 54 objects of the sample, in both LW2 and LW7 filters. Errors were estimated using a bootstrapping technique. This technique is based on a Monte Carlo simulation: new brightness profiles are obtained by perturbation of the measured profile, using a normal distribution of the same width as the error of the measured point. New fit parameters are determined for each one of the simulated profiles (30 simulations) and the uncertainty of each parameter is computed as the standard deviation of the resulting values. We calculated the fluxes integrating all the emission contained in each fitted component and in the total fit, for both LW2 and LW7 filters. As an additional check point, we verified that the resultant flux from the total fit was at least $\sim 95\%$ of the total measured flux. All fluxes and its errors are reported in Table 3. We found that bulges are only needed in the case of three galaxies: Mrk 3, MGC6-30-15, and Mrk 841, which are morphologically classified as S0 or elliptical (see Table 1). 27 galaxies were fitted using a PSF plus an exponential component, 14 with PSF plus exponential component plus bar, 4 with exponential component plus bar, 3 with PSF plus exponential component plus ring, 2 with PSF plus bar plus ring, and one with exponential component only. The galaxies NGC 7592 and ESO137-G34 can not be fitted because of their double nucleus, NGC 5929 because of the proximity of its companion (the starburst galaxy NGC 5930), and the QSO HS1700+6416 because of their high $z=2.736$. For these four galaxies without profile decomposition, total fluxes were obtained by means of aperture photometry, using the PHOT task, within the IRAF environment.

We show in Fig. 1 examples of brightness profile decomposition, fitting different morphological components, in both LW2 (left panels) and LW7 (right panels) filters. The origin of X-axis corresponds to the center of fitted isophotes, and distance from this origin is given in pixels, being the pixel size of $3''$.

3.2. Comparison with previous studies

The main interest of our work is focused into a reliable measurement of the nuclear flux, as well as its relative value to the total flux for each galaxy. Once we have obtained the fluxes for each morphological component, reported in Table 3, the first task we accomplished was the comparison of our results with the previous ones obtained from the same data sample and reported by Clavel et al. (2000) (hereafter C00). Here we recall that in C00, nuclear fluxes were obtained by integrating within a circular aperture of 3 pixel radius ($9''$) for point-like sources, and within an aperture of 4.5 pixels ($13.''5$) for extended ones. In order to account for the emission in the wings of the PSF they also corrected by a factor 1.23. We note that this photometric correction makes sense for point sources, although their effect is not clear on extended sources like most of our targets are. We present in Fig. 2 the difference between our total values and C00 measurements, normalized to our total fluxes. It can be seen that for most of the galaxies, our total fluxes are underestimated about 10% compared with C00 ones. This might be due to the introduction of the correction for the PSF wings in C00 fluxes and not in our values, which is compensated by the fact that our measurements extended all over the detector, as opposite to C00, which uses a limited aperture. On the contrary, for large galaxies, as for example NGC 5033, NGC 5674, NGC 1241, and NGC 3982, our flux measurements are much higher than those reported by C00. This discrepancy is due to the use of a 4.5 pixels aperture by C00 in clearly extended sources, resulting in underestimations of $\sim 60\%$. We also present in Fig. 2 the comparison between our nuclear fluxes and the C00 values, normalized to C00 values. In this case all our nuclear fluxes are lower than C00 ones, since we have subtracted the contribution of the galaxy to the nuclear flux, and moreover the radius of our Gaussian PSF is smaller than 3 pixels (the aperture employed by C00 for point-like sources). Note that for Sy1 galaxies our values are in better agreement with C00, due to the fact that the compact nuclear component is dominant relative to the total galaxy emission. Summarizing, we believe that the differences found between our flux measurements and those reported by C00 justify the need of a brightness profile decomposition in order to get a more accurate determination of the nuclear flux.

4. Results

4.1. Nuclear vs total emission

Once we have performed the profile decomposition we can measure the relative contribution of the nuclear source to the total emission for 54 objects of our sample. Note that for 7 galaxies our profile decomposition does not include a nuclear component (see Table 2),

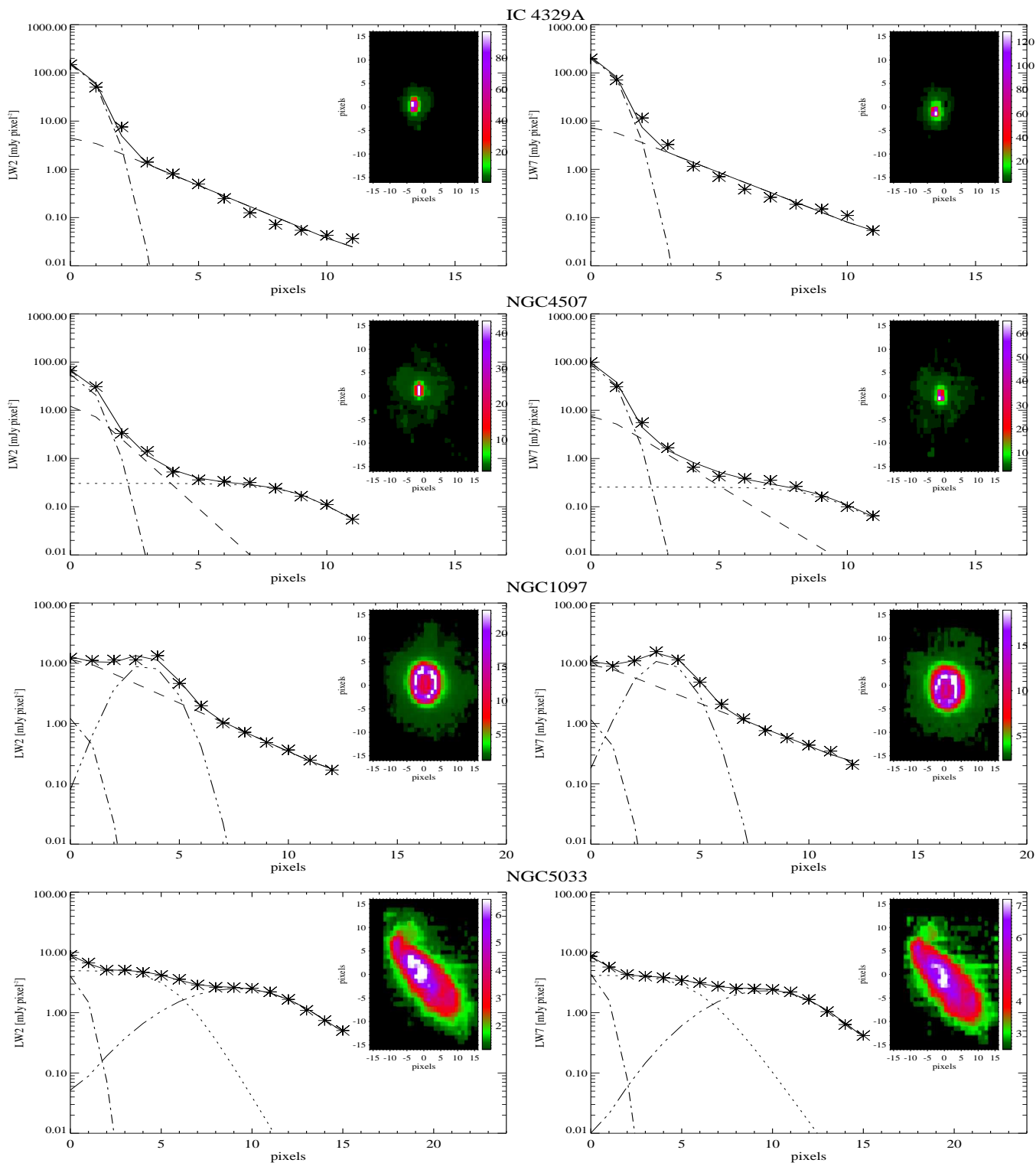


Fig. 1.— Brightness profiles of the Sy1 galaxy IC 4329 in both LW2 and LW7 filters, fitted by an exponential component (dashed line) plus a Gaussian PSF (dot-dashed line). Filled line is the final fit. The same for the Sy2 galaxy NGC 4507, fitted by an exponential component (dashed line) plus a Gaussian PSF (dot-dashed line) and a flat bar (dotted line); for the Sy1 galaxy NGC 1097, fitted by an exponential component (dashed line) plus a Gaussian PSF (dot-dashed line) and a nuclear ring (double-dot-dashed line); and finally for the Sy2 galaxy NGC 5033, fitted by a Gaussian PSF (dot-dashed line) plus a flat bar (dotted line) and a ring (double-dot-dashed line). Figures 1.1 - 1.50 are available in the electronic edition of the journal.

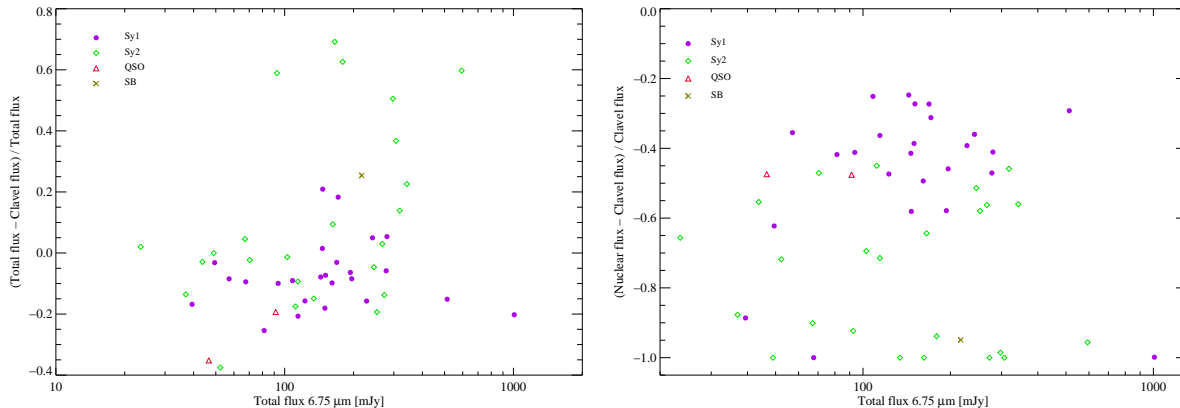


Fig. 2.— Left panel: comparison of our total fluxes (see Table 3) with the reported ones in Clavel et al. (2000). Filled circles represent Sy1 (25 in total), open diamonds Sy2 (24 in total), open triangles QSOs (2 in total), and the starburst galaxy, NGC 701, is represented by a cross. NGC 1144 and Mrk 789 fluxes were not reported by C00. Right panel: the same comparison, but for our nuclear fluxes.

which includes 6 Sy2, namely NGC 1144, Mrk 3, NGC 1667, NGC 5728, and NGC 5953, plus the Sy1 Mrk 841 (it is an elliptical galaxy and the central component is better fitted with a bulge solely). We show in Fig. 3 the ratio of nuclear to total emission at 6.75 and 9.62 μm , respectively. It can be seen in both cases that there is a clear difference between the ratios for the Seyfert types 1 and 2. In fact, the median of the ratio between nuclear and total fluxes for type 1 galaxies are 0.61 and 0.49, in the 6.75 and 9.62 μm filters, respectively. These values are both 0.14 for type 2 galaxies. In case of type 2 objects, most of them are grouped around the lowest values of the nuclear vs total flux ratio, whereas for type 1, the maximum number of objects are located around or above the value 0.5. We have applied the Kolmogorov–Smirnov test to check the significance level probability of the apparent difference between Sy1 and Sy2 distributions. We found that in both wavelength ranges, the nuclear to total flux distributions for Sy1 and Sy2 are different in a 99.9%.

We conclude that nuclear emission in the mid-infrared is a significative contribution of the total flux in Sy1 galaxies, whereas for Sy2 other components overcome the nuclear emission. This result is consistent with the unification model predictions, since the orientation of the molecular torus for type 1 Seyfert would be face-on with respect to our line of sight whereas for type 2 would be edge-on. Similar results have been found previously at different spectral ranges (Yee 1983; Alonso-Herrero et al. 1996).

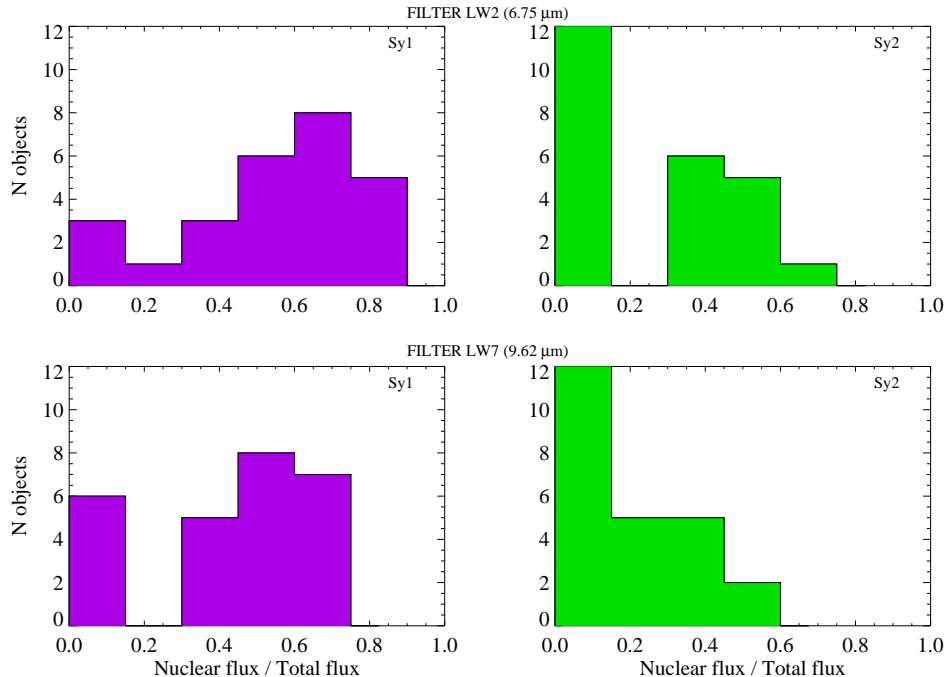


Fig. 3.— Histograms of nuclear vs total emission for Sy1 (left panels) and Sy2 galaxies (right panels) at $6.75 \mu\text{m}$ (top plots) and $9.62 \mu\text{m}$ (bottom plots). Note that for Sy2 galaxies, most of them are concentrated around the lowest values of this ratio, what does not happen in the case of Sy1.

4.2. Nuclear and host galaxy mid-infrared colors

We have studied the mid-infrared color distributions for both the nuclear and the host galaxy emission. The colors of host galaxies are computed after subtracting the nuclear to the global emission. We represent in Fig. 4 the $9.62/6.75 \mu\text{m}$ color histograms for both the nuclear and the host galaxy emission, for each Seyfert type. The nuclear $9.62/6.75 \mu\text{m}$ color distributions look very similar for both types, being the median values 1.14 and 1.02 for Sy1 and Sy2, respectively. We have performed a Kolmogorov-Smirnov test, obtaining a probability of 18%, which indicates that both color distributions are not statistically different. Previous works (Spinoglio & Malkan 1989; Fadda et al. 1998; Kuraszekiewicz et al. 2003; Alonso-Herrero et al. 2003; Lutz et al. 2004; Rigby et al. 2004) have found similar observed spectral energy distributions (SEDs) in the mid-infrared ($\lambda > 5 \mu\text{m}$) for Sy1 and Sy2 galaxies, These results are in conflict with the predictions of many compact torus models (Pier & Krolik 1992; Granato & Danese 1994; Efstathiou & Rowan-Robinson 1995; Granato et al. 1997), that has promoted the search of a more distributed or complex geometry of the absorbing material around the AGN (Nenkova et al. 2002; Fritz et al. 2006; Elitzur & Shlosman 2006; Ballantyne et al. 2006).

Despite the small number of galaxies in our sample and the proximity of the bands analysed, we can conclude that the nuclear mid-infrared emission seems to be very similar and relatively flat in both types of Seyfert galaxies.

On the other hand, the color distributions of host galaxies look different, being those of type 1 redder than those of type 2 (median values of 2.00 and 1.41, respectively). The Kolmogorov-Smirnov test confirms that both distributions are different with a probability larger than 99%. This result seems to contradict the core idea of Seyfert unification scheme, which predicts no much influence of the host galaxy to determine the type of active nucleus. In the same line of our result, Hunt & Malkan (1999) pointed out that Sy1 could be older, more evolved than Sy2, since they are found more commonly in earlier morphological types.

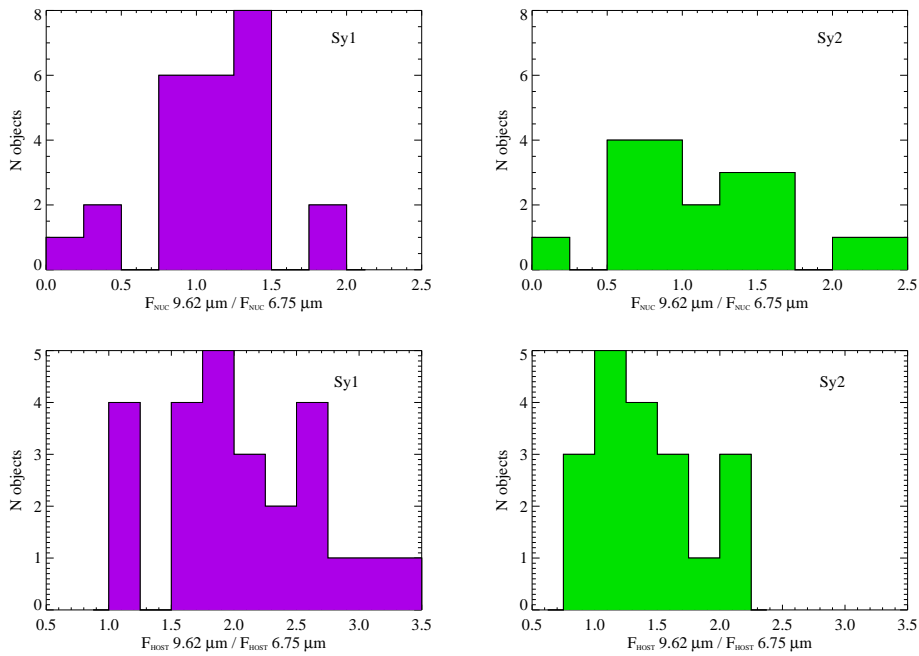


Fig. 4.— 9.62/6.75 μm colors for nuclear fluxes (top panels) and for host galaxy fluxes (bottom). Left histograms represent Sy1 and right ones, Sy2.

4.3. The radio/mid-infrared correlation in our sample

A well-known correlation between global far-infrared and radio emission from galaxies apply to a wide range of Hubble types (Fitt et al. 1988; Hummel et al. 1988; Wunderlich et al. 1987). The most natural explanation for such correlation is related to star-formation activity. In addition, Elbaz et al. (2002); Gruppioni et al. (2003) found that it can be also

extended to the mid-infrared range although with larger dispersion. Thus, the study of the radio/far-infrared correlation in active galactic nuclei turns out to be an useful tool for studying the starburst-AGN relationship. A priori, the presence of nuclear radio activity not related to supernova remnants should introduce departures from the mentioned correlation. Roy et al. (1998) reported that Seyfert galaxies also display the radio/far-infrared correlation, although with a larger scatter than non-active galaxies. They also found that Seyfert with compact radio cores tend to deviate from the correlation, contrary to those without compact cores. However, they noted that the correlation does not improve after subtraction of the compact radio emission.

We have investigated the presence of the radio/mid-infrared correlation in our sample of Seyfert galaxies. The radio data were taken from those available in the literature. Most of them (data of 32 galaxies) come from the sample observed by Rush et al. (1996) at 20 cm using the VLA⁵. The resolution (~ 1.5) of these radio data samples the emission of large scales in the galaxy, namely ~ 35 kpc at the median distance of the sample. From here and in all later sections, we will present results only using the LW2 filter, but we have always checked that the results obtained with both filters are practically the same. We have excluded two galaxies from subsequent analysis because their behaviour deviates from the rest of the sample. They are identified as NGC 4593 (its radio flux is a lower limit) and Mrk 335 (a S0 galaxy with a low radio emission likely due to be an early type galaxy). The luminosity-luminosity scatter diagram is presented in Fig. 5. A linear correlation appears in log-log scale, with a slope of 1.07 and a coefficient $r = 0.88$ ⁶. Similar correlations are found when the data are fitted for types 1 and 2, separately (see Fig. 5). The highest correlation coefficient ($r = 0.95$) appears when only Sy2 are considered. In addition, we have applied a non-parametric correlation test, such as the Spearman's rank correlation test. The results indicate that the correlation is significant ($p < 0.01$) in all cases (all galaxies, and Sy1 and Sy2, separately).

We have also explored the existence of such a correlation between the same radio data and our estimations of the nuclear mid-infrared emission. The luminosity scatter diagram is presented in Fig. 6. In this case, the correlation appears worse ($r \simeq 0.68$) than when

⁵For another 6 objects (Mrk 789, NGC 4579, ESO141-G55, NGC 4593, Mrk 509, and NGC 701) we have used VLA measurements at 20 cm, reported by different authors (Ulvestad & Wilson 1984; Condon et al. 1998; Ho & Ulvestad 2001; Wadadekar 2004).

⁶In order to verify that the correlation is not a distance effect, we have performed a test by upsetting in a random way the redshifts (z) of galaxies. If the linear correlation is merely a distance effect, it should be maintained with any z distribution. In our case, the correlation disappears when the distance distribution is changed, confirming that the observed correlation is not a distance effect.

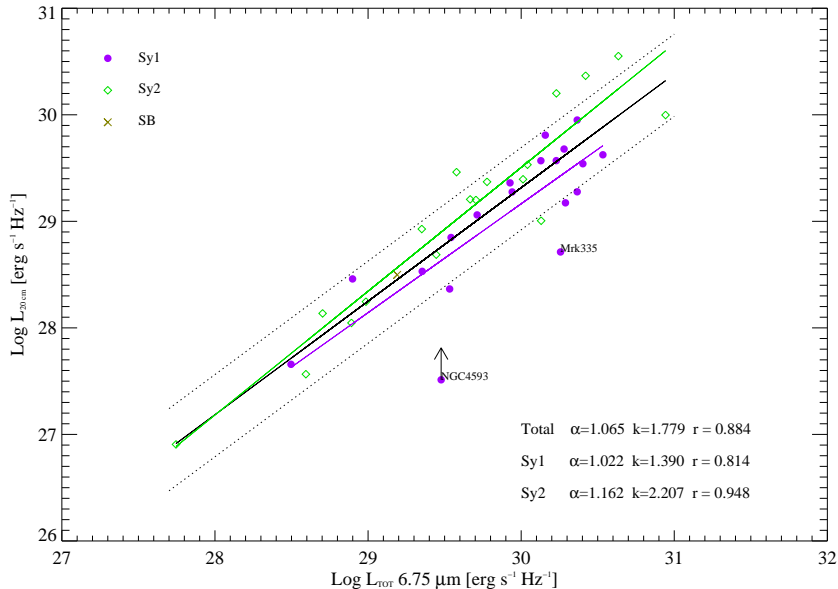


Fig. 5.— Radio luminosity (L_{20cm}) versus mid-infrared global luminosity (L_{TOT} 6.75 μm). Filled circles represent Seyfert 1 (19 in total), open diamonds Seyfert 2 (18 in total) and the cross the starburst galaxy, NGC 701. The continuous black line represents a linear fit to all data, the dashed lines correspond to the limits of the correlation at one σ . The values of α and k are derived from the expression $L_{20cm}/10^{28} = k \cdot (L_{TOT}/10^{29})^\alpha$ and are given explicitly in the legend. Separate fits to types 1 and 2 data are also presented.

global mid-infrared luminosity is considered. Moreover, the correlation becomes distant from linear in log-log space, being the slopes different from unity (see values in Fig. 6). We also noticed that the correlation slightly improves when only Sy2 galaxies are considered. The less luminous galaxies (mostly Sy2) display an excess of radio luminosity compared to their nuclear mid-IR luminosity, indicating that most of the radio emission in these objects is not related to nuclear processes. Summarizing, the global radio emission seems to be related closely to AGN activity in the most nuclear-infrared luminous galaxies (mostly Sy1), whereas for the less luminous the radio emission would be more related to non-nuclear stellar processes. In this respect it is worth to mention the result of Baum et al. (1993), who found that extra-nuclear (several kpc) radio emission, similar to the lobes of powerful radio galaxies, appears frequently in galaxies whose properties are dominated either by an AGN or a starburst.

According to our results, we claim that for the less radio luminous galaxies (mostly Sy2), radio emission is more related to stellar processes, given the fact that most of the mid-infrared emission does not come from the nuclear region. However, for the more luminous galaxies (mostly Sy1), the correlation could be attributed to extended radio emission which

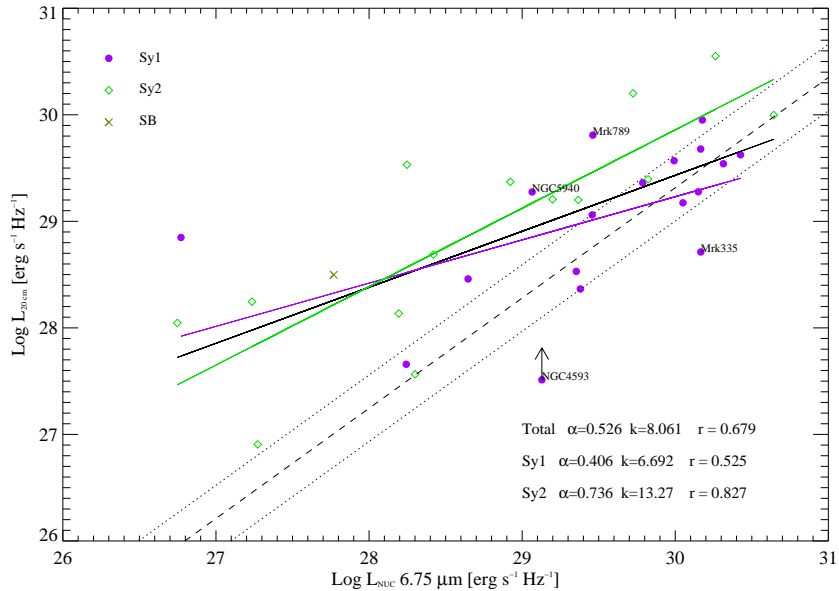


Fig. 6.— Radio luminosity (L_{20cm}) versus mid-infrared nuclear luminosity (L_{NUC} $6.75 \mu m$). The meaning of symbols is the same as in Fig. 5. The continuous line represents the fit to all galaxies, the dashed line represents the correlation using global mid-IR luminosity, from Fig. 5. The corresponding fits to Sy1 and Sy2 data separately, are also represented.

is somewhat related to the presence of the AGN as claimed by Baum et al. (1993) and indirectly by Roy et al. (1998).

4.4. Comparison among X-rays and mid-infrared emission

The hard X-ray (2-10 keV) spectral region is of particular interest for the study of AGN. It provides a direct view to the central engine and it is believed to be a reasonable isotropic indicator of the bolometric luminosity of the nuclei. On contrast, in the simple unified models, the mid-infrared emission is expected to vary as a function, not only of the AGN luminosity, but also of the distribution of the obscuring matter along the viewing direction of the observer. As a result of this, the comparison of the mid-infrared versus the hard X-ray measurements constitutes an important test for unification models.

Here, we compare our mid-infrared measurements with the hard X-ray fluxes compiled by Lutz et al. (2004), obtained from various literature sources, taken by different satellites (e.g. ASCA, BeppoSAX, Chandra, XMM-Newton). They reported measurements of 35 objects which are also included in our sample, from which only 27 galaxies have intrinsic or absorption-corrected values. We represent in Fig. 7 the histograms corresponding to

observed hard X-ray fluxes for Sy1 and Sy2, plus absorption corrected hard X-ray fluxes for Sy2. Given the fact that the hard X-ray emission in Sy2 galaxies is commonly strongly absorbed, it makes sense to consider the intrinsic, instead than the observed, hard X-ray fluxes. For those cases in which absorption corrected fluxes are not provided we adopt the observed flux as a lower limit. In this section we do not refer to the total infrared flux since hard X-ray emission is expected to be uniquely related to nuclear emission.

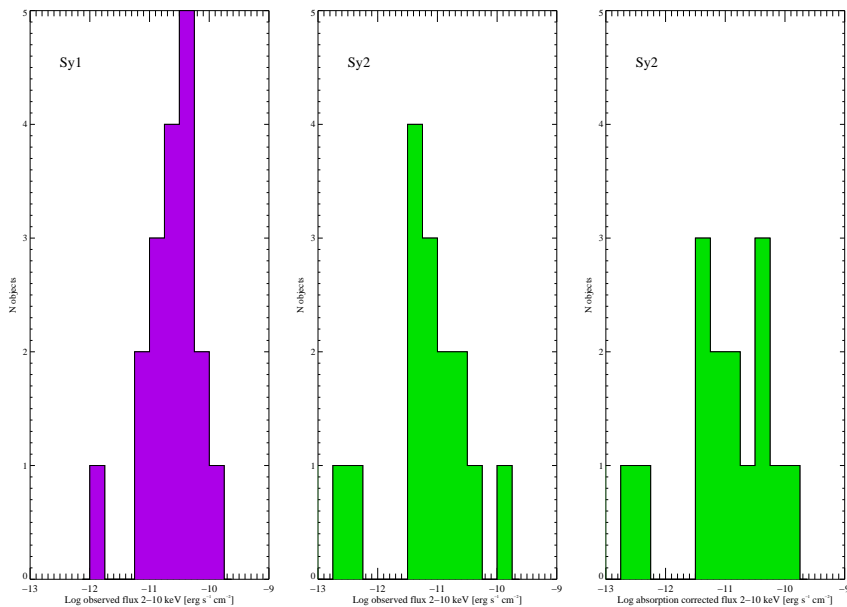


Fig. 7.— Histograms of observed hard X-ray fluxes for Sy1 (left), Sy2 (center), and absorption corrected hard X-ray fluxes for Sy2 (right).

We have also looked for a correlation between X-ray and mid-infrared luminosities (see Fig. 8). The data corresponding to all galaxies display a linear correlation of slope 0.8 with correlation coefficient $r = 0.83$. We noticed that a good correlation appears between X-ray and nuclear mid-infrared luminosities for type 1 nuclei ($\alpha = 0.97$ and $r = 0.95$). However, the data for type 2 nuclei present higher dispersion ($\alpha = 0.56$ and $r = 0.58$), showing lower mid-infrared luminosities relative to their X-ray luminosities. We have also applied the Spearman’s rank correlation test, finding that the correlation is significant when all galaxies and only type 1 nuclei are considered. We have checked that this correlation is not a distance effect by upsetting in a random way the redshift distribution of the galaxies.

The ratio of hard-X ray to nuclear mid-infrared emission appears larger in the case of type 1 nuclei ($\langle \log(L_{intr}^X/L^{MIR}) \rangle = -1.62 \pm 0.35$), than in the case of type 2 nuclei ($\langle \log(L_{intr}^X/L^{MIR}) \rangle = -1.19 \pm 0.67$). Both distributions appear significantly different according to the Kolmogorov-Smirnov test. We have excluded the galaxies NGC1386 and

NGC7674 due to their extremely low ratios, which in addition are lower limits.

The difference in the ratios for Sy1 and Sy2 appears contradictory to that has been claimed by Lutz et al. (2004) and Horst et al. (2006). Nevertheless, we expect to find different results when we compare with the work of Lutz et al. (2004), since they have extracted the nuclear emission by spectral decomposition of very large aperture data. We have checked that their estimations of the AGN contribution are largely overestimated compared to our measurements of the nuclear component. In the case of Horst et al. (2006), they have obtained very high resolution data in the mid-infrared range but their sample is very reduced. The small dispersion claimed by Horst et al. (2006) could be due to the limited number of galaxies included.

Our results are in qualitative agreement with the predictions of unification models. In case of type 1 nuclei we would see direct emission from the nucleus at any wavelength range. In type 2 nuclei the intrinsic hard X-ray emission would be similar, *i.e.*, after absorption correction, to type 1. The mid-infrared emission coming from a dusty torus would depend on the viewing angle as a function of the optical depth of the obscuring structure. The predictions vary drastically for different models. The initially proposed torus models by Pier & Krolik (1992) predict large variation for both Seyfert type in the mid-infrared range. However, more recent clumpy torus models do not predict large offset between both Seyfert types (Nenkova et al. 2002; Hönig et al. 2006). This variation will be larger for shorter wavelengths where the innermost part of the torus dominates, and will be attenuated for longer wavelengths where the outermost parts dominate. This may be one of the reasons to explain why we detect large difference in the X-ray to mid-infrared ratio for types 1 and 2, contrary to that has been found by previous authors using a longer wavelength filter (Horst et al. 2006).

4.5. The mid-infrared properties of hidden broad-line region Seyfert 2 and narrow-line Seyfert 1 galaxies

According to the unification scheme of Seyfert galaxies each Sy2 galaxy should have a hidden broad-line region (HBLR), as found in the prototypical NGC 1068 (Antonucci & Miller 1985). However, spectropolarimetric surveys of complete samples of Sy2 galaxies show that hidden type 1 nuclei have been detected in less than 50 % of the galaxies from the CfA and 12 μm samples (Lumsden & Alexander 2001; Moran et al. 2000; Tran 2001, 2003). These objects with failed detection of a type 1 nuclei are known as non-hidden broad-line region (NHBLR) Sy2 galaxies. The non-detection of broad lines could be explained in the case of an edge-on line of sight or in the absence of an electron scattering region (Miller & Goodrich

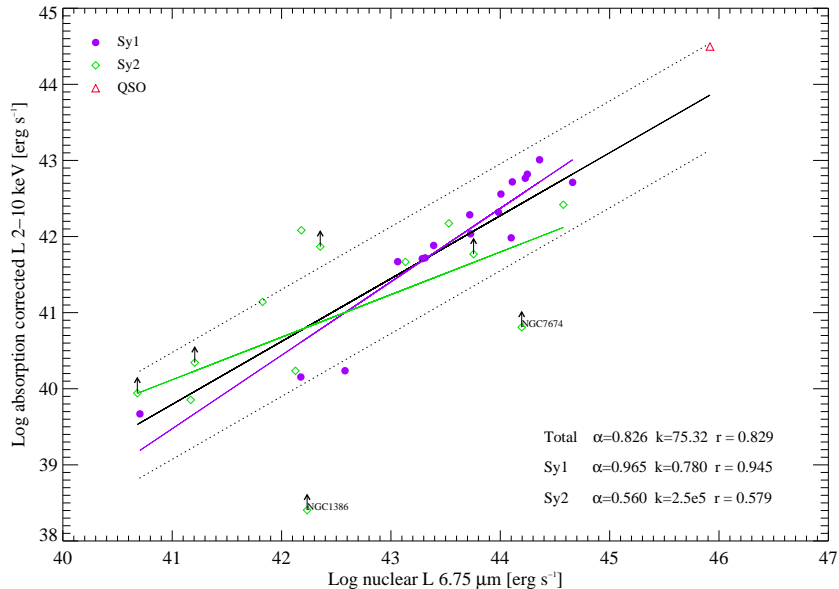


Fig. 8.— Absorption corrected hard X-ray luminosities versus nuclear $6.75 \mu\text{m}$ luminosities. Continuous line in black is the total fit and dotted lines correspond to one σ limits. Filled circles represent Sy1 (17 in total), open diamonds Sy2 (13 in total), and the QSO H 1821+643 is represented by an open triangle. Fits to Sy1 and Sy2 data are represented too. Observed hard X-ray luminosities are represented as lower limits when no N_H data is reported.

1990; Taniguchi & Anabuki 1999). However, some large-scale characteristics of the HBLR galaxy population are not shared by the non-HBLR population. The HBLR galaxies display distinctly higher radio power relative to their far-infrared output and hotter dust temperature ($F_{25\mu\text{m}}/F_{60\mu\text{m}}$ color), compared to the NHBLR Sy2 galaxies (Tran 2003). The NHBLR galaxies also appear systematically as weaker radio sources than their HBLR counterparts (Thean et al. 2001). The level of obscuration, as measured by the Balmer decrement, is indistinguishable between both types of Sy2 as well as the high level of starlight domination (Moran et al. 2000). Thus, the relative number of HBLR and non-HBLR galaxies cannot be explained by different orientations, challenging the unification scheme (Tran 2001, 2003; Lumsden & Alexander 2001). These results strongly support the existence of two intrinsically different populations of Sy2 galaxies: one harbouring an energetic, hidden Sy1 nucleus with a broad-line region and the other, "true" Sy2 galaxies, with a weak or absent type 1 nucleus and a strong, likely dominating starburst component (Tran 2003).

Three galaxies from Tran (2003) with spectropolarimetric confirmed HBLR are included in our initial sample of 57 AGNs, namely NGC 4388, NGC 7674, and IR 05189-2524, and also seven NHBLR, namely Mrk 266, NGC 1144, NGC 1241, NGC 1386, NGC 1667, NGC 3982, and NGC 5929. We have investigated possible differences in the mid-infrared properties

segregating both types of Sy2 galaxies in our sample. We add two Sy2 galaxies to the Tran (2003) ones, namely IC 4397 and NGC 7592, and other Seyfert types for which we have found far-infrared data in the literature (Pérez García & Rodríguez Espinosa 2001). We present in Fig. 9 the variation of the ratio between our mid-infrared nuclear and total fluxes versus the far-infrared color $F_{25\mu\text{m}}/F_{60\mu\text{m}}$. The nuclear versus total emission ratios of the HBLR are among the highest values for Sy2. On the contrary, for NHBLR these ratios are among the lowest values. The ratio of the nuclear versus total flux is below 0.02 in NGC 1241 and NGC 3982, and does not exceed 0.5 in Mrk 266, IC 4397, and NGC 1386. For the galaxies NGC 1144 and NGC 1667 we could not identify a central unresolved source, which could be associated with the presence of an AGN. NGC 5929 and NGC 7592 are excluded from this analysis because their nuclear emission cannot be isolated because of its close-by companion, and because of its double nucleus, respectively, due to our limited spatial resolution. Both galaxies appear in Fig. 9 in order to show their far-infrared colors.

Tran (2003) found that the far-infrared colors $F_{25\mu\text{m}}/F_{60\mu\text{m}}$ compared to the radio flux can be used as a good discriminant between HBLR and NHBLR (Fig. 4 in Tran 2003). We present a similar diagram in Fig. 10 for the galaxies in our sample. Radio fluxes (20 cm) are the same used in Section 4.3. Despite the low number of objects, it appears that recognized HBLR Sy2 galaxies are located in the upper-right corner, whereas NHBLR galaxies tend to occupy the bottom-left corner of the diagram. As a result of the use of Figs. 9 and 10 as diagnostic diagrams we can propose new NHBLR candidates. For instance, IC 4397 and NGC 7592 are located in the left-bottom quadrant of Fig. 10, and the former also shows a low nuclear to total flux ratio. These facts would support the classification of IC 4397 and NGC 7592 as possible NHBLR Sy2 nucleus.

It is interesting to look at the position of intermediate Seyfert type galaxies in Fig. 10. Tran (2001) only reports pure Sy2 data, but in Fig. 10 we are including Sy1.8 and Sy1.9 too. All the three Sy1.9 have low $S_{20\text{cm}}/F_{60\mu\text{m}}$ and $F_{25\mu\text{m}}/F_{60\mu\text{m}}$ ratios, corresponding to the NHBLR region. Sy1.8 galaxies occupy random positions in the diagram.

Zhang & Wang (2006) suggest that NHBLR Sy2 are the counterparts of Narrow Line Seyfert 1 (NL Sy1) viewed at larger angles. The NL Sy1 class is characterized for very narrow Balmer lines [H_β FWHM $\leq 2000 \text{ km s}^{-1}$], strong [Fe II] lines (Osterbrock & Pogge 1985), and violent variability in soft X-rays (Boller et al. 1996). We have looked for galaxies in our sample classified by them as NL Sy1 and we found three: Mrk 335, Mrk 766, and NGC 4051, whose fluxes are reported in Table 3. In our diagrams (Figs. 9 and 10) these galaxies occupy the same region as Sy1 and HBLR Sy2. According to our view this result contradicts the hypothesis of Zhang & Wang (2006).

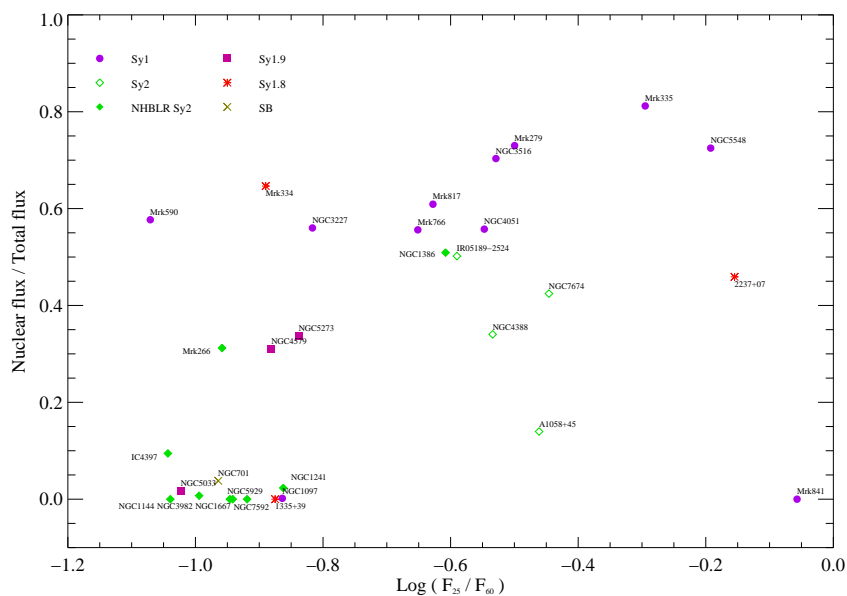


Fig. 9.— Nuclear/total mid-infrared flux ratio versus the far-infrared color $F_{25\mu\text{m}}/F_{60\mu\text{m}}$ for galaxies in our sample. NHBLR are shown as filled diamonds and confirmed HBLR as open diamonds. Circles represent Sy1, squares Sy1.9, asterisks Sy1.8, and the starburst galaxy is marked with a cross. IC 4397 and NGC 7592 are represented as NHBLR type 2 nuclei based only in their position in this diagram.

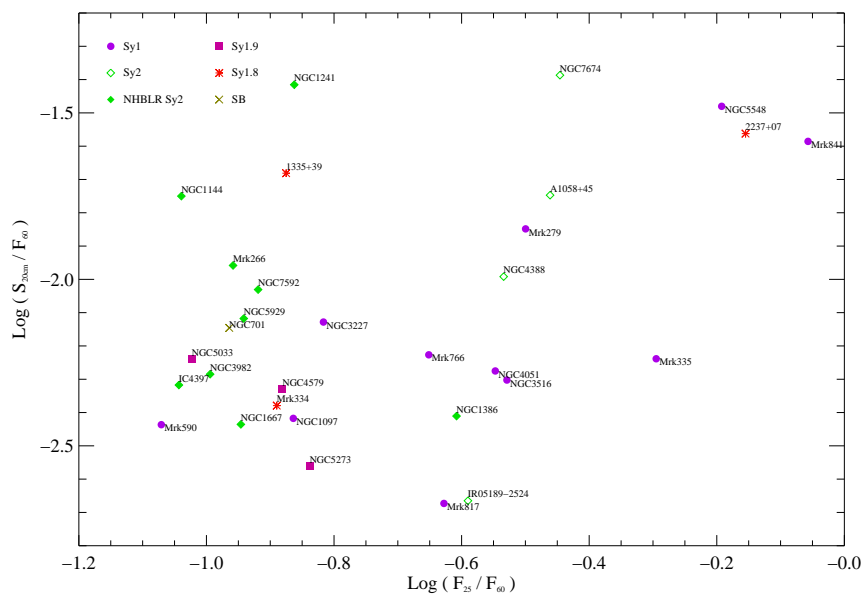


Fig. 10.— Ratio of radio flux density $S_{20\text{cm}}$ and far-infrared flux $F_{60\mu\text{m}}$ as a function of $F_{25\mu\text{m}}/F_{60\mu\text{m}}$ for galaxies of our sample. IC 4397 and NGC 7592 are represented as NHBLR type 2 nuclei based only in their position in this diagram. Symbols are the same as in Fig. 9

5. Conclusions

We have presented and analyzed mid-infrared data of a sample of Seyfert galaxies obtained with the instrument ISOCAM, being able to separate the nuclear and extended contributions to the total emission. The following results were found:

- The nuclear emission in the mid-infrared is a significant contribution to the total flux in Sy1 galaxies whereas for Sy2 other components overcome the nuclear emission. This result is consistent with the unification model predictions.
- The mid-infrared color distribution of the host galaxies of Sy1 appears redder than that of Sy2, whereas the nuclear mid-infrared emission seems to be more similar in both types of Seyfert galaxies, being also relatively flat.
- The global radio emission of Seyfert galaxies seems to be related closely to AGN activity in the most nuclear-infrared luminous galaxies (mostly Sy1), whereas for the less luminous (mostly Sy2) the radio emission would be more related to non-nuclear stellar processes.
- The luminosity–luminosity scatter diagram between hard X-ray and mid-infrared emission seems to indicate a good correlation between the two quantities, at least in the case of type 1 nuclei. The ratio between the intrinsic hard X-ray and the nuclear mid-infrared emission presents large scatter and slightly larger values for type 2 Seyfert galaxies. These results seem to be consistent with the presence of a clumpy dusty torus surrounding the active nucleus.
- The mid-infrared properties of HBLR and NHBLR nuclei appear different. The nuclear to total flux ratios of the HBLR objects are among the highest values for Sy2. On the contrary, for NHBLR these ratios are among the lowest values. A diagram representing the mid-infrared nuclear to total emission ratio versus the far-infrared colors seems to be a useful tool to segregate both types of Sy2 nuclei.

We thank the anonymous referee for his very useful comments that led to the improvement of our work. This research has made use of the NASA/IPAC Extragalactic Database (NED) which is operated by the Jet Propulsion Laboratory, California Institute of Technology, under contract with the National Aeronautics and Space Administration. This publication makes use of data products from the Two Micron All Sky Survey, which is a joint project of the University of Massachusetts and the Infrared Processing and Analysis

Center/California Institute of Technology, funded by the National Aeronautics and Space Administration and the National Science Foundation. We thank the anonymous referee for his very useful comments that led to the improvement of our work.

REFERENCES

- Alonso-Herrero, A., Quillen, A. C., Rieke, G. H., Ivanov, V. D., & Efstathiou, A. 2003, *AJ*, 126, 81
- Alonso-Herrero, A., Ward, M.J., & Kotilainen, J.K. 1996, *MNRAS*, 278, 902
- Antonucci, R. R. J. & Miller, J. S. 1985, *ApJ*, 297, 621
- Antonucci, R. 1993, *ARA&A*, 31,473
- Ballantyne, D. R., Shi, Y., Rieke, G. H., Donley, J. L., Papovich, C., & Rigby, J. R. 2006, *ApJ*, 653, 1070
- Baum S. A., O’Dea C. P, Dallacassa, D., De Bruyn A. G., & Pedlar, A. 1993, *ApJ*, 419, 553
- Boller, Th., Brandt, W. N., & Fink, H. 1996, *A&A*,305,53
- Buta, R. 1996, in *IAU Colloq.*, 157, *Barred Galaxies*, ed. R. Buta, D. A. Crocker, & B. G. Elmegreen (ASP Conf. Ser. 91; San Francisco: ASP), 11
- Cesarsky, C., et al. 1996, *A&A*,315,32
- Chen, L.-H. & Wang, J.-M. 2004, *ApJ*,614,101
- Clavel, J., et al. 2000, *A&A*,357,839
- Condon, J. J., Cotton, W. D., Greisen, E. W., Yin, Q. F., Perley, R. A., Taylor, G. B., & Broderick, J. J. 1998, *AJ*,115,1693
- Efstathiou, A., & Rowan-Robinson, M. 1995, *MNRAS*, 273, 649
- Elbaz, D., Cesarsky, C. J., Chanial, P., Aussel, H., Franceschini, A., Fadda, D., & Chary, R. R. 2002, *A&A*, 384, 848
- Elitzur, M., & Shlosman, I. 2006, *ApJ*, 648, L101
- Fadda, D., Giuricin, G., Granato, G. L., & Vecchies, D. 1998, *ApJ*, 496, 117
- Feigelson, E. D. & Berg, C. J. 1983, *ApJ*, 269, 400

- Fitt, A. J., Alexander, P., & Cox, M. J. 1988, MNRAS, 233, 907
- Fritz, J., Franceschini, A., & Hatziminaoglou, E. 2006, MNRAS, 366, 767
- Granato, G. L., & Danese, L. 1994, MNRAS, 268, 235
- Granato, G. L., Danese, L., & Franceschini, A. 1997, ApJ, 486, 147
- Gruppioni, C., Mignoli, M., & Zamorani, G. 1999, MNRAS, 304, 199
- Gruppioni, C., Pozzi, F., Zamorani, G., Ciliegi, P., Lari, C., Calabrese, E., La Franca, F., & Matute, I. 2003, MNRAS, 341, L1
- Hönig, S. F., Beckert, T., Ohnaka, K., & Weigelt, G. 2006, A&A, 452, 459
- Horst, H., Smette, A., Gandhi, P., & Duschl W.J. 2006, A&A, 457, L17
- Hunt, L.K., & Malkan, M.A. 1999, ApJ, 516, 660
- Hunt, L.K., & Malkan, M.A. 2004, ApJ, 616, 707
- Jaffe, W., Meisenheimer, K., Röttgering, H. J. A., et al. 2004, Nature, 429, 47
- Jedrzejewski, R. I. MNRAS, 226, 747
- Kessler, M. F., et al. 1996, A&A, 315, 27
- Krabbe, A., Böker, T., & Maiolino, R. 2001, ApJ, 557, 626
- Kuraszkiewicz, J. K. 2003, ApJ, 590, 128
- Ho, L. C., & Ulvestad, J. S. 2001, ApJS, 133, 77
- Hummel, E., Davies, R. D., Pedlar, A., Wolstencroft, R. D., & van der Hulst, J. M. 1988, A&A, 199, 91
- Laor, A., et al. 1997, ApJ, 477, 93
- Lemke, D., et al. 1996, A&A, 315, 64
- Lumsden, S. L. & Alexander, D. M. 2001, MNRAS, 328, 32
- Lutz, D., Maiolino, R., Spoon, H. W. W., & Moorwood, A. F. M. 2004, A&A, 418, 465
- Malkan, M. A., Gorjian, V., & Tam, R. 1998, ApJS, 117, 25

- Melo, V. P., Pérez García, A. M., Acosta-Pulido, J. A., Muñoz-Tuón, C., & Rodríguez Espinosa, J. M. 2002, *ApJ*, 574, 709
- Miller, J. S. & Goodrich, R. W. 1990, *ApJ*, 355, 456
- Moran, E. C., Barth, A. J., Kay, L. E., & Filippenko, A. V. 2000, *ApJ*, 540, L73
- Nenkova, M., Ivezić, Ž., Elitzur, M. 2002, *ApJ*, 570, L9
- Oliver, S., et al. 2000, *MNRAS*, 316, 749
- Osterbrock, D. E. & Pogge, R. W. 1985, *ApJ*, 297, 166
- Pérez García, A. M. & Rodríguez Espinosa, J. M. 2001, *ApJ*, 557, 39
- Piccinotti, G., Mushotzky, R. F., Boldt, E. A., Holt, S. S., Marshall, F. E., Serlemitsos, P. J., & Shafer, R. A. 1982, *ApJ*, 253, 485
- Pier, E. A., & Krolik, J. H. 1992, *ApJ*, 401, 99
- Prieto, M., Gottesman, S. T., Aguerri, J.-A.L., & Varela, A.-M. 1997, *AJ*, 114, 1413
- Rigby, J. R., et al. 2004, *ApJS*, 154, 160
- Rowan-Robinson, M., & Crawford, J. 1989, *MNRAS*, 38, 523
- Roy, A. L., Norris, R. P., Kesteven, M. J., Troup, E. R., & Reynolds, J. E. 1998, *MNRAS*, 301, 1019
- Rush, B., Malkan, M. A., & Edelson, R. A. 1996, *ApJ*, 473, 130
- Siebenmorgen, R., Haas, M., Krügel, E., & Schulz, B. 2005, *A&A*, 436, L5
- Spinoglio, L., & Malkan, M. A. 1989, *ApJ*, 342, 83
- Taniguchi, Y. & Anabuki, N. 1999, *ApJ*, 521, 103
- Thean, A., Pedlar, A., Kukula, M. J., Baum, S. A., & O’Dea, C. P. 2001, *MNRAS*, 325, 737
- Tran, H. D. 2001, *ApJ*, 554, 19
- Tran, H. D. 2003, *ApJ*, 583, 632
- Ulvestad, J. S., & Wilson, A. S. 1984, *ApJ*, 285, 439
- Ulvestad, J. S., & Wilson, A. S. 1989, *ApJ*, 343, 659

Ulvestad, J. S., & Ho, L. C. 2001, ApJ, 558, 561

Wadadekar, Y. 2004, A&A, 416, 35

Wang, J.-M., Szuszkiewicz, E., Lu, F.-J., & Zhou, Y.-Y. 1999, ApJ, 522, 839

Wunderlich E., Wielebinski R., Klein U. 1987, A&AS, 69, 487

Yee, H. K. C. 1983, ApJ, 473, 473

Zhang, E.-P. & Wang, J.-M. 2006, accepted 2006 June 5 by ApJ

TARGET	Morphology	Type	z	Exptime (s)	Start Time (UT)
NGC1097	RSB(r)b	Sy1	0.00425	516	01 01 1997 02:20:48
NGC1125	SAB0	Sy2	0.01100	516	01 02 1998 13:42:51
NGC1144	RSApec	Sy2	0.02885	516	13 07 1997 05:44:46
NGC1241	SB(rs)b	Sy2	0.01351	516	04 01 1998 15:03:35
Z 1335.5+3925	S?	Sy1.8	0.02009	516	09 06 1996 12:45:19
NGC1386	SB(s)0+	Sy2	0.00289	516	27 01 1998 02:50:27
NGC1566	RSAB(rs)bc	Sy1	0.00499	516	18 05 1997 18:08:52
NGC1667	SAB(r)c	Sy2	0.01517	516	02 10 1997 21:32:21
Mrk266	pec	Sy2/SB	0.02786	516	04 05 1996 16:04:24
Mrk279	S0	Sy1.5	0.02940	514	05 02 1996 07:26:57
NGC3227	SAB(s)pec	Sy1.5	0.00386	516	25 04 1996 04:32:37
Mrk334	pec/HII	Sy1.8	0.02196	516	12 12 1996 00:59:23
Mrk335	S0/a	Sy1.2	0.02564	516	12 12 1996 01:29:13
NGC3516	RSB(s)0	Sy1.5	0.00884	524	12 03 1996 11:32:22
NGC3982	SAB(r)b	Sy2	0.00370	524	08 04 1996 06:14:36
3C382	BLRG	Sy1	0.05787	514	16 02 1996 18:30:26
Mrk3	S0:	Sy2	0.01351	516	04 09 1997 11:12:01
NGC4051	SAB(rs)bc	Sy1.5	0.00242	516	09 05 1996 09:36:57
IC4329A	SA0+	Sy1.2	0.01605	514	14 02 1996 16:25:00
NGC4388	SA(s)b	Sy2	0.00842	516	09 07 1996 06:18:36
IC4397	S?	Sy2/HII	0.01474	514	07 02 1996 19:08:30
NGC4507	SAB(s)ab	Sy2	0.01180	514	04 02 1996 12:06:42
NGC4579	SAB(rs)b	Sy1.9/LINER	0.00507	516	13 07 1996 00:03:03
NGC4593	RSBb(rs)b	Sy1	0.00900	516	14 07 1996 06:20:04
NGC5033	SA(s)c	Sy1.9	0.00292	516	25 06 1996 12:13:25
Mrk509	Compact	Sy1.2	0.03440	516	18 10 1996 03:03:22
NGC526A	S0pec?	Sy1.5	0.01922	516	24 11 1996 03:13:59
NGC5273	SA(s)0	Sy1.9	0.00352	516	25 06 1996 11:51:23
NGC5548	RSA(s)0/a	Sy1.5	0.01717	514	07 02 1996 16:57:22
NGC5674	SABc	Sy1.9	0.02492	514	07 02 1996 14:05:36
NGC5728	RSAB(r)a	Sy2	0.00930	514	07 02 1996 08:49:23
Mrk590	SA(s)a	Sy1.2	0.02638	516	03 07 1997 15:11:27
NGC5929	Sab: pec	Sy2	0.00831	514	05 02 1996 13:31:51
NGC5940	SBab	Sy1	0.03405	514	07 02 1996 15:06:16
NGC5953	SAa pec	Sy2/LINER	0.00656	514	07 02 1996 16:24:58
Mrk673	S?	Sy2/LINER/HII	0.03651	514	07 02 1996 19:55:02
NGC701	SB(rs)c	SB	0.00610	516	18 12 1997 00:35:41
NGC7314	SAB(rs)bc	Sy1.9	0.00474	516	29 04 1996 12:42:14
NGC7592	S0+pec	Sy2	0.02444	516	15 11 1996 15:56:53
NGC7603	SA(rs)b pec	Sy1.5	0.02952	516	18 05 1996 05:47:11
Mrk766	RSB(s)a	Sy1.5	0.01293	516	02 06 1996 04:17:32
NGC7674	SA(r)bc pec	Sy2/HII	0.02906	516	28 05 1996 06:39:23
Mrk789	Irregular	Sy1/HII	0.03145	516	16 12 1996 12:51:04
Mrk817	SBc	Sy1.5	0.03145	514	05 02 1996 14:04:02
Mrk841	E	Sy1.5	0.03620	514	07 02 1996 15:54:02
A 1058+45	Sa	Sy2	0.02908	516	18 04 1996 09:51:17
Ark 120	Sb/pec	Sy1	0.03273	516	20 08 1997 13:05:38
ESO137-G34	SAB(s)0/a?	Sy2	0.00916	514	09 02 1996 08:31:18
ESO141-G55	Sc	Sy1	0.03600	524	04 03 1996 18:04:15
FAIRALL9	S	Sy1	0.04702	516	06 05 1996 09:28:16
H 1821+643		QSO/Sy1	0.29700	514	05 02 1996 10:11:07
HS0624+6907		QSO	0.37000	516	04 09 1997 09:06:18
HS1700+6416		QSO	2.73574	826	18 10 1996 19:52:33
IR 05189-2524	pec	Sy2	0.04256	516	18 10 1997 00:57:35
IR 12495-1308	Sa	Sy1	0.01463	516	19 12 1996 11:29:20
IR 22377+0747	SBa	Sy1.8	0.02460	516	18 05 1996 09:26:28
MCG+8-11-11	SB0	Sy1.5	0.02048	516	14 10 1997 23:51:53
MGC-6-30-15	E-S0	Sy1.2	0.00775	514	14 02 1996 17:51:30

Table 1: Morphological classification of the galaxies, Seyfert type and spectroscopic redshift (obtained from the NASA/IPAC Extragalactic Database, *NED*).

Table 2. Fitted parameters and errors for each galaxy in both LW2 and LW7 filters: PSF intensity (in mJy), exponential component length scale, bar length scale, bar falling slope, ring radial offset, and ring width (all parameters except the PSF intensity are given in pixels, being the pixel size of 3"). * Mrk 3, MGC-6-30-15 and Mrk 841 have been fitted by bulges (they appear in the bar parameters columns in order to avoid enlargement of the table), bulge length scale and Sersic law index are given.

GALAXY	PSF int.		Exp. length scale		Bar length scale		Bar falling slope		Ring radial offset		Ring width	
	LW2	LW7	LW2	LW7	LW2	LW7	LW2	LW7	LW2	LW7	LW2	LW7
NGC1097	1.21±1.31	1.16±1.30	2.70±0.10	3.07±0.26	3.41±0.11	3.27±0.08	0.75±0.11	0.79±0.18
NGC1125	14.2±4.5	9.67±2.63	14.7±4.9	14.7±4.9	2.16±1.43	3.10±0.85	0.62±0.35	0.33±0.24
NGC1144	7.59±2.11	7.50±2.10	2.98±0.56	2.88±0.08	0.06±0.02	0.06±0.05
NGC1241	1.87±1.45	1.72±0.81	9.45±0.46	10.3±3.1	1.44±0.21	2.01±1.32	1.14±0.72	1.00±0.68	0.88±0.37	1.00±0.50
Z 1335.5	1.34±0.06	1.32±0.06
NGC1386	46.7±2.4	43.8±1.7	2.24±0.05	3.16±0.07
NGC1566	18.2±5.8	7.95±2.53	1.42±0.20	1.52±0.11	10.0±2.0	10.0±2.0	2.00±0.40	2.00±0.40
NGC1667	2.10±0.20	2.62±0.62	7.63±0.64	8.71±0.65	1.19±0.18	1.18±0.22
Mrk266	13.3±5.4	13.7±5.3	1.21±0.13	1.76±0.17
Mrk279	22.2±2.0	29.3±6.7	1.84±0.10	1.18±0.09
NGC3227	58.2±6.7	54.6±5.5	1.29±0.15	1.30±0.20	0.40±0.10	0.40±0.10	13.2±2.6	13.0±3.0
Mrk334	26.8±3.0	17.1±3.9	0.99±0.06	0.88±0.05
Mrk335	43.3±4.8	34.6±5.0	1.23±0.10	1.20±0.10
NGC3516	59.6±8.2	76.3±10.3	1.45±0.11	1.42±0.09
NGC3982	1.50±0.20	2.36±0.34	5.30±0.30	5.54±0.23	1.69±0.07	1.75±0.05
3C382	15.0±3.1	17.5±4.2	1.32±0.19	2.02±0.41
Mrk3	(8.77±0.59)	(8.97±0.33)	(2.40±0.10)	(2.02±0.09)
NGC4051	58.4±9.1	65.0±15.8	13.0±3.0	12.9±3.4	0.30±1.10	0.29±1.02	0.75±0.28	0.80±0.30
IC4329A	155±32	209±32	1.98±0.13	2.10±0.10
NGC4388	44.2±3.6	38.8±4.9	19.6±4.5	20.0±5.0	2.50±0.40	2.20±0.30	0.30±0.10	0.30±0.10
IC4397	2.37±0.26	1.69±0.25	3.37±0.11	3.70±0.10
NGC4507	55.8±8.4	89.4±16.2	0.90±0.20	1.34±0.15	9.34±0.44	9.57±0.59	0.90±0.20	0.95±0.24
NGC4579	12.0±1.3	16.4±1.7	2.01±0.07	2.77±0.16
NGC4593	32.9±13.1	43.5±8.0	0.99±0.26	1.02±0.11
NGC5033	4.05±0.49	4.38±0.44	5.54±0.24	5.92±0.33	0.87±0.15	1.04±0.18	9.13±0.34	9.60±0.30	3.06±0.16	2.70±0.10
Mrk509	44.1±5.3	42.8±7.8	1.44±0.16	1.20±0.10
NGC526A	32.8±2.7	35.2±5.9	1.64±0.15	1.52±0.15
NGC5273	2.96±0.46	2.90±0.80	3.21±0.33	2.92±0.35
NGC5548	40.6±3.3	42.2±4.1	1.58±0.08	1.49±0.07
NGC5674	1.97±1.47	2.59±1.93	1.97±0.19	1.28±0.31	8.00±2.00	7.50±1.00	1.00±0.10	2.00±0.10
NGC5728	6.06±3.45	6.00±3.00	0.60±0.50	0.60±0.50	0.65±0.16	0.61±0.07
Mrk590	31.5±8.9	47.7±11.1	2.67±0.30	3.52±0.40
NGC5940	2.38±0.26	1.58±1.04	32.0±1.0	32.5±0.7	4.97±0.21	3.19±2.20	0.06±0.17	1.50±0.70
NGC5953	1.50±0.80	2.11±3.25	2.43±0.86	2.18±1.12	0.25±0.14	0.44±0.29

Table 2—Continued

GALAXY	PSF int.		Exp. length scale		Bar length scale		Bar falling slope		Ring radial offset		Ring width	
	LW2	LW7	LW2	LW7	LW2	LW7	LW2	LW7	LW2	LW7	LW2	LW7
Mrk673	7.59±3.80	2.00±2.00	1.76±1.92	5.20±4.60	1.26±0.92	1.57±0.71	0.68±0.26	0.46±0.25
NGC701	5.57±1.22	2.12±0.95	4.18±0.16	4.55±0.19
NGC7314	8.21±4.99	8.72±2.52	7.30±4.30	7.00±4.00	1.00±0.10	1.30±0.30	0.58±0.21	0.05±0.03
NGC7603	32.9±1.9	29.3±1.7	2.60±0.40	2.60±0.40
Mrk766	33.5±8.2	42.4±10.6	4.50±1.90	4.54±1.89	1.00±0.10	1.05±0.99	0.60±0.20	0.61±0.24
NGC7674	42.4±6.2	58.6±16.2	2.13±0.15	2.51±0.28
Mrk789	6.79±5.36	3.36±3.59	6.00±8.00	5.89±7.68	2.30±0.90	2.31±0.92	0.63±0.40	0.63±0.40
Mrk817	27.7±3.9	53.1±4.9	1.23±0.08	1.51±0.08
Mrk841	(5.72±0.83)	(6.56±0.61)	(1.87±0.40)	(1.66±0.28)
A 1058+45	1.96±0.37	3.11±1.13	2.94±0.17	3.18±0.23
Ark 120	43.5±24.7	17.8±13.7	1.59±0.60	1.41±0.18
ESO141-G55	22.6±2.9	21.7±11.4	13.0±3.1	15.0±4.0	0.61±1.13	0.50±0.90	0.85±0.30	0.61±0.29
FAIRALL9	47.3±9.2	53.5±9.9	1.33±0.16	1.47±0.10
H 1821+643	21.2±1.6	27.4±2.1	1.36±0.06	1.28±0.05
HS0624+6907	12.3±2.1	14.6±2.5	1.35±0.14	1.47±0.15
IR 05189-2524	47.1±10.1	71.5±22.8	3.19±0.39	3.41±0.58	1.85±0.13	1.87±0.85	0.02±0.04	0.18±0.22
IR 12495-1308	7.25±0.56	10.7±1.1	4.06±0.46	3.51±0.44
IR 22377+0747	7.51±3.93	6.30±3.30	0.89±0.32	0.65±1.82	8.95±3.11	9.11±2.17	0.29±1.65	0.56±1.21
MCG+8-11-11	54.7±14.7	47.9±21.0	0.84±0.18	0.73±0.11	12.3±0.5	12.5±0.5	0.54±0.73	0.53±0.72
MGC-6-30-15	43.1±16.3	54.1±11.5	(7.35±0.75)	(8.13±0.37)	(1.12±0.27)	(1.00±0.10)

Table 3. Fluxes (in mJy) obtained by an integration of the emission of each individual component (PSF profile, exponential component, bar and ring) plus the total fit. For Mrk 3, MGC6-30-15, and Mrk 841, which have been fit to bulges, total fluxes are given, like in the case of ESO137-G34, NGC5929, NGC7592, and HS1700+6416, whose total fluxes were obtained by aperture photometry.

GALAXY	PSF flux		Exp. comp. flux		Bar flux		Ring flux		Total flux	
	LW2	LW7	LW2	LW7	LW2	LW7	LW2	LW7	LW2	LW7
NGC1097	1.70±1.60	3.10±2.90	448±10	490±23	543±113	555±86	1008±29	1054±32
NGC1125	38.1 ±6.3	25.5 ±4.4	7.82±0.45	28.0±1.0	26.0±21.0	31.0±25.0	70.4 ±9.6	83.0±5.0
NGC1144	89.0±5.0	86.2±1.4	70.0±4.0	62.0±9.0	166±4	155±5
NGC1241	4.14±2.27	2.40±0.90	155±21	166±80	22.0±9.0	17.4±1.9	179±11	197±10
Z 1335.5+3925	47.4±2.8	56.7±2.8	49.0±3.1	57.3±2.8
NGC1386	125±5	117±3	120±2	172±2	246±8	287±5
NGC1566	48.6±11.3	11.6±2.7	73.0±11.0	128±9	29.1±1.3	113±8	147±13	265±19
NGC1667	47.0±8.0	69.0±10.0	260±24	262±21	307±10	334±11
Mrk266	36.0±10.0	36.0±9.0	78.0±16.0	89.0±18.0	114±14	126±13
Mrk279	59.4±3.3	79.0±11.0	22.7±1.4	54.0±7.0	81.3±4.6	133±14
NGC3227	156±13	146±12	80.0±14.0	140±5	48.0±7.0	57.6±0.7	278±14	355±17
Mrk334	72.0±5.0	46.0±8.0	40.0±5.0	77.0±10.0	111±7	128±9
Mrk335	117±9	93.0±10.0	31.0±4.0	81.0±8.0	144±12	176±13
NGC3516	160±15	203±20	66.0±5.0	121±8	228±20	332±26
NGC3982	2.14±0.26	4.31±0.53	279±11	306±9	297±10	327±7
3C382	40.0±5.7	46.0±12.0	18.0±3.0	21.0±15.0	57.2 ±7.3	67.3 ±10.6
Mrk3	134±7	245±15
NGC4051	156±17	174±34	45.7±0.8	51.0±8.0	280±23	361±30
IC4329A	418±45	563±45	116±14	203±15	513±65	753±66
NGC4388	117±8	103±18	192±9	183±3	36.0±12.0	65.0±21.0	342±11	350±16
IC4397	6.33±0.42	4.50±0.60	60.4±1.3	93.7 ±2.2	67.1±1.1	99.9±2.1
NGC4507	148±17	241±35	92.0±16.0	111±20	71.9±3.2	68.0 ±6.0	318±17	404±25
NGC4579	31.8±2.2	43.4 ±3.7	71.1±2.3	91.0 ±3.0	103±3	135±5
NGC4593	87.0±23.0	117±21	108±29	128±28	194±17	240±14
NGC5033	10.5±0.6	11.5 ±0.5	220±6	205±7	364±9	325±11	594±5	541±4
Mrk509	118±8	115±11	34.0±4.0	83.0±10.0	151±12	194±16
NGC526A	88.4 ±4.5	94.0 ±12.0	23.0 ±2.0	51.0 ±4.0	108±7	144±11
NGC5273	7.91 ±0.95	7.60 ±1.50	14.9 ±0.9	25.0 ±2.0	23.5 ±1.3	34.0 ±2.3
NGC5548	109±6	113±7	43.8 ±2.6	102±6	150±8	225±11
NGC5674	2.92±1.41	6.88 ±3.32	51.0±5.0	40.0±8.0	38.0±6.0	63.3±2.2	92.0±9.0	113±5
NGC5728	41.0±6.0	122±2	121±48	74.1±5.9	162±12	200±10
Mrk590	84.0 ±18.0	124±21	57.0 ±7.0	181±14	146±23	303±25
NGC5929	12.4±0.1	13.0±0.1
NGC5940	5.24 ±0.77	4.17±1.68	8.46 ±0.66	28.7 ±1.1	25.0±5.0	46.0±14.0	39.4±1.9	81.0±5.0

Table 3—Continued

GALAXY	PSF flux		Exp. comp. flux		Bar flux		Ring flux		Total flux	
	LW2	LW7	LW2	LW7	LW2	LW7	LW2	LW7	LW2	LW7
NGC5953	86.0±28.0	80.0±48.0	186±79	143±70	272±4	223±2
Mrk673	20.0±9.0	4.10±1.90	2.72±2.04	21.0±7.0	30.0±11.0	49.0±21.0	52.3±6.0	75.0 ±7.0
NGC701	8.24±1.28	3.09±0.98	210±4	212±5	217±5	215±5
NGC7314	18.0±6.0	23.0±6.0	112±19	104±3	33.0±8.0	22.0±5.0	166±10	163±11
NGC7592	161±1	143±1
NGC7603	87.9±2.2	78.5±10.1	28.8±0.4	90.0±11.0	114±4	168±4
Mrk766	89.6±10.8	113±18	21.3±0.6	54.0±17.0	55.9±5.2	95.0±9.0	161±17	260±23
NGC7674	113±10	157±30	147±8	222±18	267±19	376±41
Mrk789	15.3 ±7.3	6.00±4.00	7.76 ±0.73	22.0±9.0	51.0±6.0	47.0±14.0	76.0±11.0	75.0 ±8.0
Mrk817	75.0±7.0	142±9	45.0±3.0	81.0 ±3.0	123±10	226±12
Mrk841	67.6 ±7.0	119±7
A 1058+45	5.17±0.79	8.19 ±1.78	31.6±1.7	45.3 ±2.1	37.0±1.7	54.6±3.7
Ark 120	96.0±33.0	26.0±13.0	73.0±29.0	147±26	171±37	180±27
ESO137-G34	138±1	94.6±0.5
ESO141-G55	61.0 ±6.0	59.0±18.0	4.75 ±1.47	6.00±1.00	30.0±12.0	83.0±35.0	93.7±5.9	136±20
FAIRALL9	126±15	144±16	40.0±7.0	85.0±12.0	169±24	229±23
H 1821+643	57.1 ±2.9	73.4 ±9.8	32.6 ±2.4	54.0 ±7.0	91.3±3.6	125±5
HS0624+6907	33.1 ±3.8	39.0 ±4.0	12.9 ±0.7	31.0 ±3.0	46.6 ±5.2	63.3 ±3.2
HS1700+6416	3.30±0.10	4.80±0.10
IR 05189-2524	127±14	193±42	62.0±5.0	78.0±4.0	68.0±13.0	134±26	253±18	411±42
IR 12495-1308	19.2 ±0.9	28.6±1.9	30.9±1.6	53.8±3.5	49.4 ±1.4	84.0±3.0
IR 22377+0747	20.1 ±5.8	16.8±4.9	18.0±3.0	28.0±4.0	8.02 ±1.97	22.1±3.3	43.7±8.7	66.0 ±19.0
MCG+8-11-11	147±29	127±44	61.0±9.0	179±18	38.3±1.8	65.9±1.2	242±21	368±33
MGC-6-30-15	115±36	144±24	196±13	272± 11

Erratum: "The mid-infrared emission of Seyfert galaxies. A new analysis of ISOCAM data¹" (AJ, 134, 2006[2007])

C. Ramos Almeida¹, A.M. Pérez García¹, J.A. Acosta-Pulido¹, and J.M. Rodríguez Espinosa¹

In our original paper (Section 4.4) we compared the ratios of hard X-ray to nuclear mid-infrared emission for Seyfert 1 and 2 nuclei, finding that both distributions appear significantly different according to the Kolmogorov-Smirnov test. We have detected a mistake in the computation of the X-ray luminosities (the lack of a 4π factor). Additionally, for two galaxies, the nuclear mid-infrared fluxes used within calculations are slightly different from the correct values which are reported in Table 3 of the original version. These mistakes affect the mentioned ratios of hard X-ray to nuclear mid-infrared emission, although does not alter the result concerning the distributions being statistically different. The correct values of these ratios are $\langle \log(L_{intr}^X/L^{MIR}) \rangle = -0.21 \pm 0.33$ for the Seyfert 1 galaxies, and $\langle \log(L_{intr}^X/L^{MIR}) \rangle = 0.17 \pm 0.62$ for the type 2 nuclei. Figure 8 has been updated with the newly computed values. We have also corrected the X-axis respect to the original figure, now being νL_ν . We have performed again the Spearman's rank correlation test, finding that the correlation is significant when all galaxies and types 1 and 2 are considered separately. It is worth to note that here we have excluded from the analysis two Seyfert 2 galaxies (NGC 1386 and NGC 7674) due to their extremely low hard X-ray luminosities, consistent with being optically thick sources. Recently, Horst et al. (2007) have estimated an intrinsic X-ray luminosity for NGC 7674 of $\log L_{intr}^X = 44.56 \text{ erg s}^{-1}$, in contrast to the non absorption-corrected value reported by Lutz et al. (2004) ($\log L_{obs}^X = 41.91 \text{ erg s}^{-1}$). Such a difference of about 2.5 dex corroborates our decision of do not include these galaxies.

In a recent job, Horst et al. (2007) have argued that our luminosity ratios are ~ 8 larger than what they have found for their well-resolved objects, claiming that our nuclear data are heavily contaminated by nuclear star formation. Instead, our new values are now of the same order of magnitude than theirs, even smaller for the case of Seyfert 2 galaxies. Therefore, we believe that despite the limited resolution of ISOCAM images, our nuclear fluxes are representative of the torus emission, and the contamination by circumnuclear star formation, although existing, is not dominant.

¹Instituto de Astrofísica de Canarias (IAC), C/Vía Láctea, s/n, E-38200, La Laguna, Tenerife, Spain. cra@iac.es, apg@iac.es, jap@iac.es, and jre@iac.es

¹Based on observations with ISO, an ESA project with instruments funded by ESA Member States (especially the PI countries: France, Germany, the Netherlands and the United Kingdom) and with the participation of ISAS and NASA.

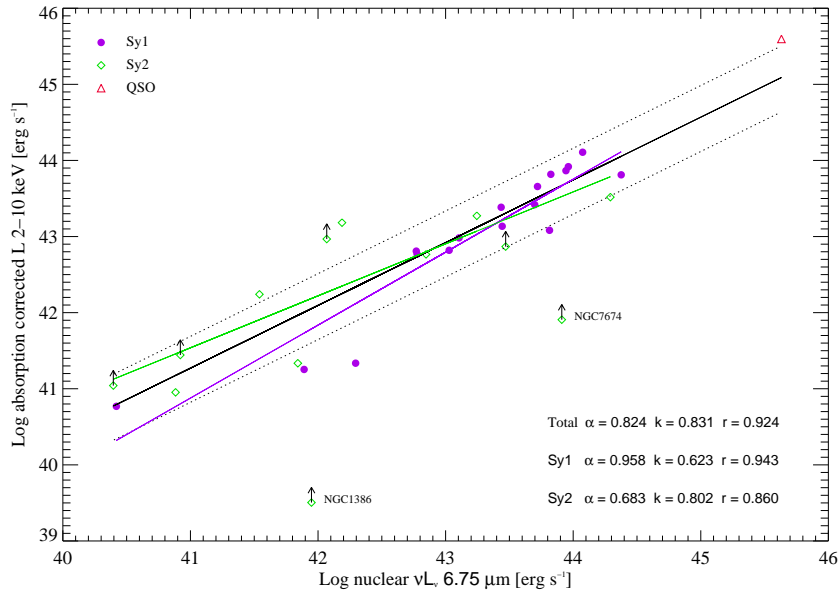


Fig. 8.— Absorption corrected hard X-ray luminosities versus nuclear $6.75 \mu\text{m}$ luminosities. Solid line in black is the total fit and dotted lines correspond to one σ limits. Filled circles represent Sy1 (17 in total), open diamonds Sy2 (13 in total), and the QSO H 1821+643 is represented by an open triangle. Fits to Sy1 and Sy2 data are represented too. Observed hard X-ray luminosities are represented as lower limits when no N_H data is reported. The galaxies NGC 7674 and NGC 1386 have not been taken into account in the correlation analysis. The values of α and k are derived from the expression $L_{intr}^X/10^{43} = k(\nu L_{\nu}^{MIR}/10^{43})^{\alpha}$.

There is a typographical mistake in Table 3 for the Point Spread Function (PSF) flux in the LW7 filter corresponding to the galaxy ESO144-G55, the correct value being 84.2 ± 2.44 mJy.

REFERENCES

- Horst, H., Gandhi, P., Smette, A., & Duschl, W. J. 2007, A&A submitted, astro-ph/0711.3734v2
- Lutz, D., Maiolino, R., Spoon, H. W. W., & Moorwood, A. F. M. 2004, A&A, 418, 465